














Venetoclax improves CD20 immunotherapy in a mouse model of MYC/BCL2 double-expressor diffuse large B-cell lymphoma

Javier Melchor ^{1,2}, Marcos Garcia-Lacarte ^{1,2,3}, Sara C. Grijalba ^{1,3}, Adrián Arnaiz-Leché ^{1,3}, Marién Pascual ², Carlos Panizo ^{3,4,5}, Oscar Blanco ⁶, Víctor Segura ^{7,8}, Francisco J. Novo ^{1,3}, Juan Garcia Valero ^{9,10}, Patricia Pérez-Galán ^{9,10}, Jose A. Martinez-Climent ^{2,3,10}, Sergio Roa ^{1,2,3,10}

To cite: Melchor J, Garcia-Lacarte M, Grijalba SC, *et al.* Venetoclax improves CD20 immunotherapy in a mouse model of MYC/BCL2 double-expressor diffuse large B-cell lymphoma. *Journal for ImmunoTherapy of Cancer* 2023;**11**:e006113. doi:10.1136/jitc-2022-006113

► Additional supplemental material is published online only. To view, please visit the journal online (<http://dx.doi.org/10.1136/jitc-2022-006113>).

Accepted 12 February 2023



© Author(s) (or their employer(s)) 2023. Re-use permitted under CC BY-NC. No commercial re-use. See rights and permissions. Published by BMJ.

For numbered affiliations see end of article.

Correspondence to

Dr Sergio Roa; sroa@unav.es

ABSTRACT

Background Approximately one-third of diffuse large B cell lymphoma (DLBCL) patients exhibit co-expression of MYC and BCL2 (double-expressor lymphoma, DEL) and have a dismal prognosis. Targeted inhibition of the anti-apoptotic protein BCL2 with venetoclax (ABT-199) has been approved in multiple B-cell malignancies and is currently being investigated in clinical trials for DLBCL. Whether BCL2 anti-apoptotic function represents a multifaceted vulnerability for DEL-DLBCL, affecting both lymphoma B cells and T cells within the tumor microenvironment, remains to be elucidated.

Methods Here, we present novel genetically engineered mice that preclinically recapitulate DEL-DLBCL lymphomagenesis, and evaluate their sensitivity *ex vivo* and *in vivo* to the promising combination of venetoclax with anti-CD20-based standard immunotherapy.

Results Venetoclax treatment demonstrated specific killing of MYC⁺/BCL2⁺ lymphoma cells by licensing their intrinsically primed apoptosis, and showed previously unrecognized immunomodulatory activity by specifically enriching antigen-activated effector CD8 T cells infiltrating the tumors. Whereas DEL-DLBCL mice were refractory to venetoclax alone, inhibition of BCL2 significantly extended overall survival of mice that were simultaneously treated with a murine surrogate for anti-CD20 rituximab.

Conclusions These results suggest that the combination of anti-CD20-based immunotherapy and BCL2 inhibition leads to cooperative immunomodulatory effects and improved preclinical responses, which may offer promising therapeutic opportunities for DEL-DLBCL patients.

BACKGROUND

Diffuse large B-cell lymphomas (DLBCL) with MYC and BCL2 co-expression not related to underlying chromosomal rearrangements, known as double-expressor lymphomas (DEL),^{1,2} account for 20%–30% of DLBCL and have been shown to develop an aggressive phenotype and poor response to standardized immuno-chemotherapeutic

WHAT IS ALREADY KNOWN ON THIS TOPIC

- ⇒ Concurrent expression of MYC and BCL2 confers dismal clinical course for diffuse large B-cell lymphoma (DLBCL), referred to as double-expressor lymphoma (DEL).
- ⇒ The antiapoptotic protein BCL2 is a promising target in hemato-oncology, which could be selectively inhibited with venetoclax (ABT-199). The therapeutic impact of BCL2 inhibition in combination immunotherapy and in the lymphoma microenvironment of DEL-DLBCL remains to be elucidated.

WHAT THIS STUDY ADDS

- ⇒ This study presents genetically engineered mice that preclinically recapitulate DEL-DLBCL lymphomagenesis, evidencing the activation of BCL2 as an early vulnerability in the lymphoma progression.
- ⇒ Venetoclax improves the efficacy of anti-CD20 immunotherapy in the long-term control of DEL-DLBCL progression, where a two-faceted effect of venetoclax results in direct killing of lymphoma B cells and intratumoral enrichment of effector CD8⁺ T cells.

HOW THIS STUDY MIGHT AFFECT RESEARCH, PRACTICE OR POLICY

- ⇒ Our preclinical evidences support the clinical rationale for incorporating venetoclax to anti-CD20-based immunotherapy for DLBCL, particularly among patients with MYC/BCL2 double-expressor status.
- ⇒ Considering the targeted and immunomodulatory effects of inhibiting BCL2, venetoclax might be further explored in novel T-cell-targeted immunotherapy combinations for DLBCL.

regimes.^{3–5} With respect to the cell-of-origin (COO) concept based on gene expression patterns in DLBCL,⁶ DEL appears to be highly correlated with the adverse prognostic subtype of activated B cell-like (ABC) DLBCL.^{3–5,7} Yet, independently of the COO

subtype, the concurrent presence of BCL2 and MYC expression confers inferior progression-free and overall survival.^{3–5, 8} TP53 alterations have been also associated with dismal clinical course,^{9–11} and when co-occurring with double MYC/BCL2 expression, loss of TP53 identifies a subset of ultrahigh-risk DLBCL.¹² Thus, there is a pressing need for the development and preclinical validation of therapeutic strategies for these patients, so that novel mouse models recapitulating human DEL-DLBCL, as presented here, become powerful *in vivo* tools for predicting combined drug responses and deciphering mechanisms of therapeutic improvement.

With the advent of BH3-mimetics to inhibit pro-survival BCL2 family proteins, there is a strong rationale to attempt disarming at least one arm of the MYC/BCL2 cooperation in DEL-DLBCL. Targeting the antiapoptotic protein BCL2 with the highly selective inhibitor venetoclax (ABT-199) has demonstrated potential to improve responses in DLBCL patients receiving R/G-CHOP (CAVALLI Phase Ib/II study, NCT02055820)^{13, 14} or dose-adjusted EPOCH-R (Phase I study, NCT03036904).¹⁵ In this regard, complementary preclinical *in vivo* studies could provide further mechanistic insights and additional supporting evidence for currently undergoing clinical trials with BCL2 inhibitors in high-grade and DEL-DLBCL. Furthermore, BCL2 is also important in T-cell homeostasis,¹⁶ and several cancer studies have demonstrated that venetoclax may lead to overall decrease in T cells^{17, 18} or even exert immunomodulatory functions by favoring T effector memory antitumoral responses.¹⁸ Here, we used venetoclax to study the effect of BCL2 inhibition on B-cell and T-cell populations within the tumor microenvironment (TME) of DEL-DLBCL mouse models and evaluated whether venetoclax could be efficiently combined with anti-CD20-based immunotherapy to improve long-term control of MYC/BCL2 co-expressing DLBCL.

METHODS

Genetically modified mice

Single-mouse strains including *p53*^F (p), *Blimp*^F (B), *IKK2ca.IRES.GFP*^{stopF} (I), *Cy1-Cre* (C) and *eYFP*^{stopF} (Y) were obtained and crossed to generate the pBIC and YC compound mice as previously described.¹⁹ To generate the new pBIC2 compound mouse model, pBIC mice were successively crossed with mice expressing human B-cell lymphoma 2 (BCL2) cDNA under the control of the Eμ immunoglobulin heavy chain enhancer (B6.Cg-Tg(BCL2)22Wehi/J; stock 002319; abbreviated as 2).²⁰ All conditional alleles were maintained as homozygous except for the *Cy1-Cre*, the *eYFP*^{stopF} reporter and the *Eμ-hBCL2* alleles, which were used as heterozygous. To promote the formation of germinal centers (GC) in splenic B cell follicles *in vivo*, 8-to-10-week-old mice were chronically immunized intraperitoneally with 10⁹ Sheep Red Blood Cells (SRBCs) every 20 days until death or enrollment in a treatment cohort. GC B cells experiencing *Cy1-Cre*-mediated recombination are marked

either: (1) by the expression of GFP under the control of an internal ribosomal entry site downstream of *IKK2ca* (when carrying the *IKK2ca.IRES.GFP*^{stopF} allele in pBIC/pBIC2 mice); or (2) by the expression of YFP, which can be activated by removal of the preceding *loxP* flanked STOP cassette (when carrying the *eYFP*^{stopF} allele in YC mice). Control and multilesion compound mice were housed in a specific pathogen-free (SPF) animal facility and were observed during 12–24 months for tumor development.

Primary cells

Mice were sacrificed at an early stage during secondary immunization (10 days after the second SRBC intraperitoneal immunization, before 100 days of age) or when moribund at the advanced lymphoma stage (ethical endpoint criteria reached and evidencing splenomegaly). At necropsy, fresh murine spleens were either fixed in 4% formaldehyde and embedded in paraffin, or submitted to mechanic disaggregation with a syringe plunger through a 70 μm cell strainer, followed by lysis of erythrocytes with ACK buffer (NH₄Cl 150 mM KHCO₃ 10 mM EDTA 0.1 mM). Then, single-cell preparations were either cryopreserved at –80°C in 90% fetal bovine serum (FBS) and 10% dimethyl sulfoxide (DMSO) or submitted to follow up procedures as fresh samples (ie, cell sorting, flow cytometry and *ex vivo* cultures).

Histopathology

Sections of paraffin-embedded formalin-fixed spleens (4 μm) were deparaffinized and stained with H&E or with specific antibodies to BCL2 (Abcam ab182858, 1:8000), GFP (Abcam ab6556, 1:1000), Ki-67 (Thermo Scientific RM9106, 1:100), or MYC (Abcam ab51154, 1:50). Of note, BCL2 antibody was able to detect both human and murine BCL2 as reported. Secondary antibodies against primary Fc were conjugated with horseradish peroxidase enzyme and developed by DAB color substrates, followed by counterstaining with hematoxylin. All slides were viewed under a light microscope and scanned using either a Leica Aperio CS2 whole-slide scanner at ×20 magnification (for an expert pathologist evaluation and confirmation of the high grade DLBCL phenotype), or a Nikon NIS Elements Microscope Imaging at ×20 and ×100 magnification (for visualization of tumors at a greater resolution and magnification).

Flow cytometry and cell sorting

The panel of antibodies indicated in online supplemental table 1 was used for flow cytometry analysis and sorting of murine immune cell populations in the spleen of pBIC or pBIC2 lymphomas at advanced stages except otherwise specified, and control YC mice of similar age. Fresh primary splenocytes were processed in a FACSAriaII sorter (BD, 3 lasers) for cell sorting, while flow cytometry data was acquired from fresh or cryopreserved samples on a CytoFLEX LX flow cytometer (Beckman Coulter) and analyzed using FlowJo software (TreeStar).

For detection of cell surface targets, splenocytes were stained for 30 min at 4°C with antibodies recognizing murine antigens except otherwise specified. Non-specific binding of antibodies was blocked using Fc Block reagent (BD Biosciences). The following combinations of antibodies were used to define populations in younger animals during secondary SRBC-immunization: germinal center B cells (B220⁺CD38^{low}Fas⁺YFP⁺ from YC control mice), and early stage tumor cells (B220⁺CD38^{high}Fas⁺GFP⁺ from pBIC or pBIC2 mice); and in the lymphoma microenvironment of moribund or age-matched control mice: normal B cells (B220⁺CD19⁺GFP⁺), advanced stage tumor cells (B220⁺/lowCD19⁺GFP⁺), plasma cells (CD138⁺YFP⁺/GFP⁺), CD4 T cells (GFPB220⁺CD3⁺CD4⁺), and CD8 T cells (GFPB220⁺CD3⁺CD8⁺). Within CD4 or CD8 cell subsets, naïve T cells were defined as CD44⁺CD62L⁺PD-1⁻, effector/effector memory T cells (E/EM) as CD44⁺CD62L⁺PD-1⁺, and central memory T cells (CM) as CD44⁺CD62L⁺PD-1⁺.

For Annexin V/7AAD apoptosis measurements, splenocytes were stained using Annexin V Binding Buffer (BD Biosciences) according to manufacturer's recommendations. For intracellular staining of GFP, γ H2AX, active caspase 3 or BCL2, splenocytes were first fixed using Cytofix/Cytoperm solution (BD Biosciences) and then permeabilized using Perm/Wash solution (BD Biosciences) according to manufacturer's recommendations, before staining with the corresponding antibodies. Particularly, both anti-human (clone 100) and anti-mouse (clone BCL/10C4) BCL2 antibodies (Biolegend) were used simultaneously for intracellular staining and the accumulated Median Fluorescence Intensity (MFI) was calculated as the sum of both mBCL2 and hBCL2 MFI values, which was further normalized to the corresponding MFI observed in normal GC B cells.

For functional T-cell analyses, splenocytes were previously stimulated with Cell Activation Cocktail (2 μ L/mL, Biolegend) and GolgiStop/GolgiPlug (BD Biosciences). After 4 hours, cells were stained with Zombie NIR Fixable dye (Biolegend) in order to assess cell viability. Intracellular staining of IFN- γ was performed similarly to previously described intracellular markers.

For intranuclear staining of MYC and TCF-1, splenocytes were processed using the Fixation/Permeabilization Concentrate and Permeabilization Buffer of the eBioscience FoxP3/transcription factor staining buffer set (Invitrogen) for 30 min at room temperature, which was followed by incubation of the splenocytes with either anti-mouse TCF-1 or a primary rabbit anti-mouse MYC unconjugated antibody and a secondary APC-labeled goat anti-rabbit IgG antibody.

For absolute cell count analysis, nucleated live cells were tabulated as the total count after dead cells, cell aggregates and debris were removed from analysis according to 7AAD signal and forward/side scatter parameters. Once naïve, CM and E/EM CD4⁺ and CD8⁺ T cell subsets were gated, a normalization factor was calculated by dividing each sample total cell count by 50,000 live lymphocytes.

A normalized cell count could finally be plotted for any given population by multiplying its cell number by the corresponding tumor normalization factor.

RNA extraction and real-time quantitative reverse transcription PCR

Total RNA was extracted from sorted cell populations using TRIzol Reagent (Invitrogen) as described in manufacturer's protocol. cDNA synthesis was performed using random hexanucleotides and PrimerScript RT Reagent Kit (TAKARA). Quantitative PCR was performed with SYBR Select (Applied Biosystems) in a VIIA7 real-time thermal cycler (Applied Biosystems) and specific primers were used (online supplemental table 2). Genes were evaluated in triplicates, normalized to the GAPDH housekeeping gene and analyzed using the $\Delta\Delta$ CT comparative method.

RNA sequencing and analysis

Total RNA was extracted from sorted lymphoma cells at advanced stages (n=3 from pBIC and n=3 from pBIC2 mice), as well as from control COO GC B cells (n=4 from YC mice), using TRIzol Reagent (Invitrogen) as described in manufacturer's protocol. RNA quality and concentration were analyzed by Agilent 2100 Bioanalyzer, followed by general transcriptome library preparation and massive sequencing performed by BGI Tech (BGI, Shenzhen, China) using the DNA Nanoball (DNBseq) platform with the single-end 50bp read option. Files have been deposited in NCBI Gene Expression Omnibus and are accessible through GEO SuperSeries accession number GSE197693.

To analyze differences in Ig gene expression, we first extracted all Ig genes from the count matrix and applied a filter to keep only rows with more than 0.5 counts per million (CPM) in 2 or more samples (292 Ig genes passed that filter). We represent oligoclonality of tumors by a heatmap of log2CPM using the R library *pheatmap*. Limma (implemented in the R library *limma*) was used to obtain differentially expressed genes between all three mouse models, first removing all Ig genes from the count matrix and applying the same filter as above (21,623 were filtered because they correspond to lncRNAs or gene predictions with very low expression, leaving 15,665 genes). We normalized the counts with the *calcNormFactors* function, which implements TMM normalization (Trimmed Mean of M-values, a weighted trimmed mean of the log expression ratios), and scaled each sample to the one with normalization factor nearest to 1 with *limma-Voom*. Genes were considered differentially expressed using an adjusted $p < 0.05$ and log2 fold change (FC) > 1 for upregulated genes and < -1 for downregulated genes. Hierarchical clustering, heatmaps, GSEA plots and GO plots were all generated in R/Bioconductor using *ggplot2*, *pheatmap* and *ClusterProfiler*. Expression levels of 18 orthologous genes previously associated with human ABC or GCB-DLBCL subtypes were used to classify our models according to their RNAseq combined score.²¹ BCL2 family members were analyzed as described²² and genes belonging to apoptosis, MYC targets and p53 pathway in the Hallmarks

category were extracted from MSigDB database (<https://www.gsea-msigdb.org/gsea/msigdb/index.jsp>).

Ex vivo treatments

Freshly collected cells after cellular disaggregation of murine spleens and erythrocyte lysis using ACK buffer were incubated in RPMI media containing 10% heat-inactivated FBS and 1% penicillin/streptomycin (complete media). For drug dose-response assays, cells were incubated in triplicates for 24 hours with serial dilutions of venetoclax (0.0024–80 μ M) (ABT-199, Chemietek) or DMSO (0%–0.01% final concentration). Cell viability was assessed through flow cytometry analysis on a CytoFLEX LX flow cytometer (Beckman Coulter) after FSC/SSC/7-AAD-based exclusion of doublets and dead cells. Percentage of viable lymphoma B cells was calculated as proportion of B220^{+/low}CD19⁺GFP⁺ cells in a given drug concentration normalized to untreated cells at the time of treatment (24 hours after plating). The half-maximal inhibitory concentration (IC50) was determined with GraphPad Prism V.9.0.2 software using the log(inhibitor) versus normalized response equation and the least squares regression fitting method during non-linear regression modeling of the data. Percentage of apoptotic AnnexinV or active caspase 3 positive cells were calculated after DMSO baseline correction by flow cytometry as indicated above. Drug effects on T cell viability were assessed by incubating fresh splenic cell suspensions with either venetoclax IC50 (6 μ M), 25 μ g of anti-CD20 (clone 5D2, isotype IgG2a, Genentech) or the combination of both for 24 hours with complete media supplemented with 10% non-inactivated rat serum, followed by T-cell specific antibody staining and flow cytometry analysis as described above.

In vivo treatments

Mice at advanced stages of the disease (ie, pBIC mice at 180 days with incipient splenomegaly) were randomly enrolled in the experimental groups and treated intraperitoneally either (1) once a week with 200 μ g of anti-mouse CD20 (10 mg/kg, clone 5D2, isotype IgG2a, Genentech); (2) twice a week with 250 μ g/dose of venetoclax (10 mg/kg, ABT-199, Chemietek); (3) with a combination of both anti-mouse CD20 and venetoclax; or (4) twice a week with 50 μ L of DMSO as the vehicle for venetoclax solubilization, corresponding to the untreated (UNT) experimental group. Treatment regimens were divided into two modalities: (1) to study overall survival, mice were treated for eight consecutive weeks and then reviewed periodically until moribund and appearance of ethical end-point criteria or (2) to study the ongoing effect of the treatment in the tumor cells and the TME, mice received four consecutive weeks of treatment (half-of-treatment duration) and then they were sacrificed and submitted to the characterization of primary tissues. Additionally, an independent cohort of pBIC mice were either untreated or treated intraperitoneally once a week with 200 μ g anti-mouse PD-1 (10 mg/kg, clone RMP1-14,

isotype IgG2a, BioXcell) for 2 weeks, before primary tissues were analyzed for IFN- γ expression.

Statistical analysis

GraphPad Prism V.9.0.2 software was used for graphic representation and most statistical analysis. Data from RNAseq were normalized and analyzed in R (V.4.0.4) as specified before. Normality and homoscedasticity were analyzed in every population. Data following a Gaussian distribution have been plotted as mean and SE, for which p values were calculated by unpaired Student's t-tests or one-way analysis of variance (ANOVA). Alternatively, for data not following a normal distribution, Mann-Whitney U tests were used and data were plotted as median and IQR. Pearson's correlation was computed assuming data followed a Gaussian distribution. Log-rank (Mantel-Cox) test was used for all survival analyses. Statistical significance in figures is indicated as follows: * (p<0.05), ** (p<0.01), *** (p<0.001), or **** (p<0.0001).

RESULTS

MYC/BCL2 co-expression is rapidly acquired in NF- κ B-driven murine lymphomas

Constitutive activation of NF- κ B is a characteristic of ABC-DLBCL,^{23 24} and NF- κ B was originally described as a potent transcriptional activator of the *Myc*^{25 26} and *Bcl2*^{27 28} promoters. Therefore, we prompted to examine MYC and BCL2 levels in normal germinal center (GC) B cells from controls (YC mice) and in lymphomas from our previously described ABC-DLBCL-like mouse model (pBIC mice)¹⁹ (figure 1A). These pBIC mice were originally engineered to model two major characteristics of ABC-DLBCL (ie, constitutive NF- κ B activation and abrogation of terminal B cell differentiation by BLIMP1 disruption), as well as loss of TP53, for arresting plasmablastic B cells in a genotoxic stage prone to DLBCL transformation.^{19 29} We observed significant co-expression of MYC and BCL2 in all murine ABC-DLBCL lymphomas studied by RNAseq (figure 1B) or immunohistochemistry (figure 1C). While the cell-cycle regulator MYC is essential for GC B cells to enter a phase of proliferative expansion,³⁰ BCL2 is normally downregulated in GCs,³¹ as we could confirm in the Ki67⁺ GC area of secondary activated follicles from control YC mice immunized with SRBC (figure 1D). Thus, to investigate early involvement of acquired BCL2 expression during GC malignant transformation, we crossed the *E μ -hBCL2* transgenic mice into the multi-lesion pBIC background (designated pBIC2) to enforce expression of human BCL2 from pre-GC stages (figure 1A and online supplemental figure S1). Constitutive expression of BCL2 in GC B cells from pBIC2 mice did not significantly accelerate pBIC lymphomagenesis triggered by *CyT^{tr}* (figure 1E), suggesting that aberrant expression of BCL2 in pBIC is already an early pro-oncogenic event. Indeed, co-expression of both MYC and BCL2 was evidenced at both early and more advanced tumor stages by real-time quantitative reverse

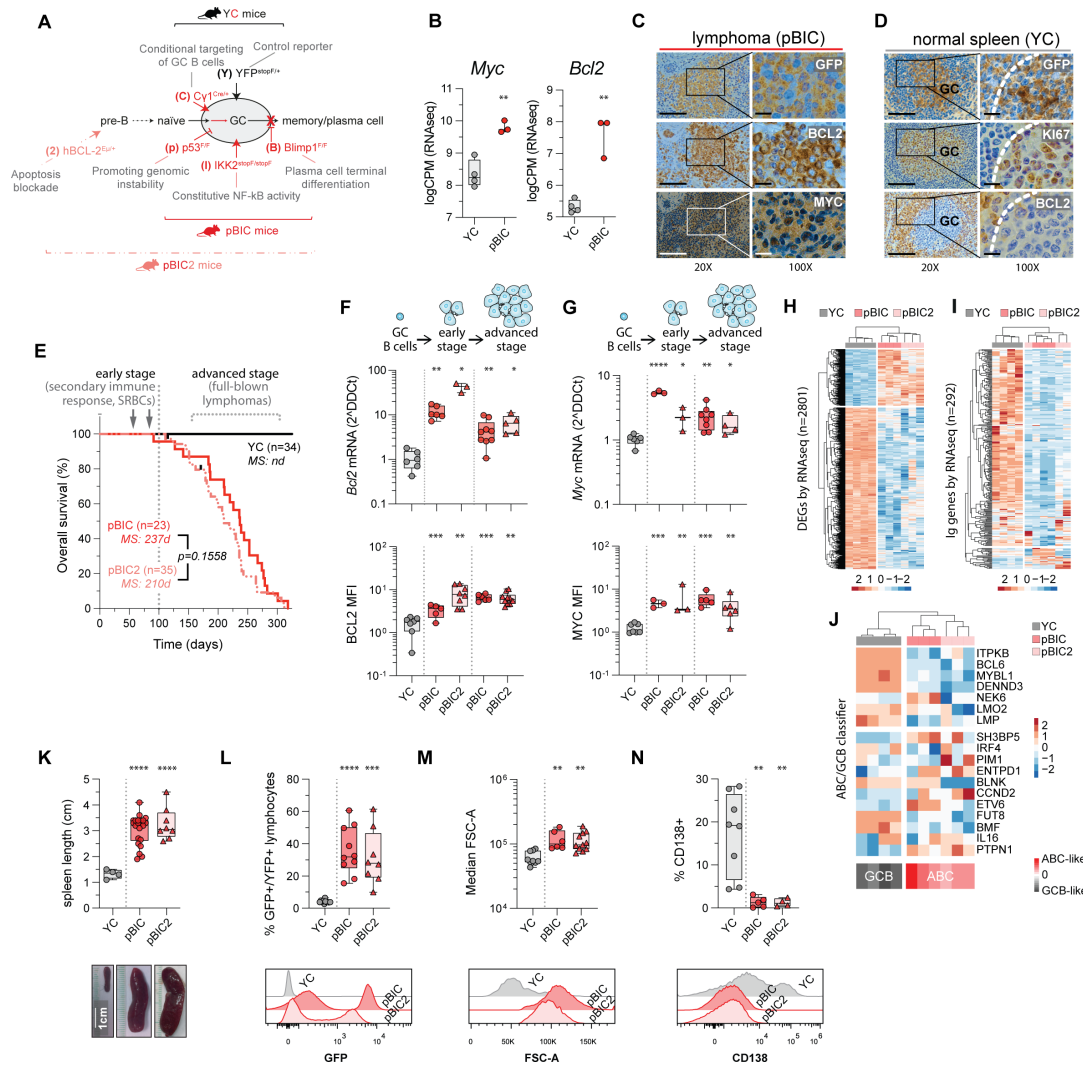


Figure 1 Spontaneous acquisition of MYC and BCL2 co-expression in mouse models of ABC-DLBCL lymphomagenesis. (A) Schematic diagram of all mutant mice and biological processes perturbed in this study. (B) Comparison of expression by RNAseq of *Bcl2* and *Myc* between normal GC B cells (B220⁺CD38^{low}FAS⁺YFP⁺) from control YC mice and B220⁺CD19⁺GFP⁺ lymphomas from pBIC mice (moribund mice around 220 days-old). (C) Representative IHC staining of GFP, BCL2 and MYC in DEL-DLBCL affecting the spleen of pBIC mice (scale bar represents 100µm and 10µm at ×20 or ×100, respectively). (D) Representative IHC staining of GFP, Ki67 and BCL2 in control YC spleens (scale bar represents 100µm and 10µm at ×20 or ×100, respectively). (E) Overall survival curves of YC control compared with both pBIC and pBIC2 multilesion lymphoma mouse models. (F, G) Expression analysis of BCL2 (F) and MYC (G) by qRT-PCR (top) and intracellular flow cytometry (bottom) of FACS-sorted GFP⁺ tumor cells compared with normal resting GC B cells. BCL2 and MYC expression were analyzed both at early stages of the disease (first three groups, mice sacrificed before 100 days of age, after secondary response to SRBC immunization, with incipient enlargement of spleen and <10% expansion of GFP⁺ tumor cells), or advanced stages of the disease (last two groups, moribund mice at a median of 220 days of age, with splenomegaly and ≥20% expansion of GFP⁺ tumor cells). (H) Heatmap of differentially expressed genes commonly altered in pBIC and pBIC2 lymphomas. (I) Heatmap of Ig-related transcripts showing decreased expression in lymphomas compared with the more diverse normal GC B cells in YC control mice. (J) RNAseq-based classifier distinguishes ABC-DLBCL subtype in the murine lymphomas. (K) Splenomegaly at advanced stages of the disease in pBIC and pBIC2 mice compared with control SRBC-immunized YC mice. (L) Comparative percentages of normal YFP⁺ or malignant GFP⁺ expansion at advanced stages of the disease (top), and representative flow cytometry profiles (bottom). (M) Comparative cellular sizes as measured by FSC-A parameter at advanced stages of the disease (top), and representative flow cytometry profiles (bottom). (N) Comparative percentages of terminally differentiated CD138⁺ plasma cells within normal YFP⁺ or malignant GFP⁺ activated B cells (top), and representative flow cytometry profiles (bottom). Circle or triangle symbols represent individual animals. Log-rank (Mantel-Cox) tests and parametric t-tests were used for statistical analysis: *p≤0.05, **p≤0.01, ***p≤0.001, ****p<0.0001.

transcription PCR and intracellular flow cytometry (figure 1F,G). Further analyses of lymphomas arising in pBIC and pBIC2 mice demonstrated similar deregulated

transcriptional programs (figure 1H), loss of BCR diversity suggestive of clonal enrichment (figure 1I) and key molecular features consistent with the ABC-DLBCL-like

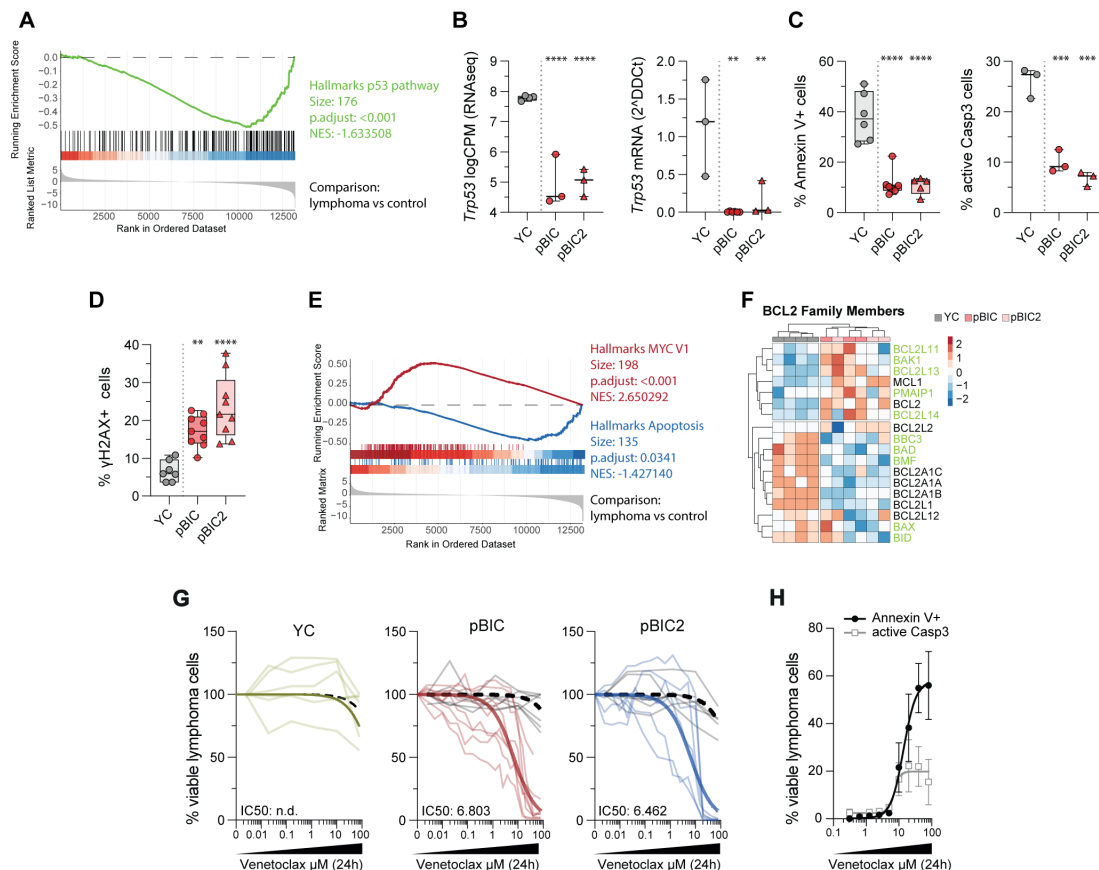


Figure 2 BCL2 inhibition licenses apoptosis of MYC/BCL2 double-expressor lymphomas. (A) GSEA plot showing that both lymphoma models analyzed together (pBIC and pBIC2 at advanced stages of the disease) recapitulate a negative enrichment of the p53 pathway over normal spleen YC control GC B cells. (B) Expression analysis of *Trp53* by RNAseq (left) and qRT-PCR (right) in FACS-sorted GFP⁺ tumor cells from pBIC or pBIC2 mice lymphomas, compared with YFP⁺ GC B cells from normal YC mice. (C) Comparative fractions of apoptotic GFP⁺ tumor cells expressing phosphatidylserine and labeled with AnnexinV (left) or cleaved caspase 3 (right) determined by flow cytometry. (D) Comparative fractions of GFP⁺ tumor cells expressing γH2AX determined by intracellular flow cytometry. (E) GSEA plot showing a positive enrichment of MYC Hallmarks (red) and a negative enrichment of Apoptosis Hallmarks (blue) in lymphomas (both pBIC and pBIC2) over control GC B cells. (F) Heatmap showing RNAseq expression changes of BCL2 family members in DEL-DLBCL models compared with normal GC B cells from YC control animals. Pro-apoptotic members are highlighted in green. (G) Normalized percentages of live 7AAD⁺B220⁺GFP⁺ tumor cells following 24-hour treatment with increasing doses of venetoclax or DMSO (black dotted line) (n≥3). (H) Percentages of live 7AAD⁺B220⁺GFP⁺ tumor cells expressing cleaved caspase 3 (light gray) or phosphatidylserine and labeled with AnnexinV (black) determined by flow cytometry following 24-hour treatment with escalating doses of venetoclax (n≥3). Circle or triangle symbols represent individual animals. Parametric t-tests, and non-linear fit analyses were used for statistical analysis: *p≤0.05, **p≤0.01, ***p≤0.001, ****p≤0.0001.

subtype as indicated by a previously validated human RNAseq-based classifier²¹ (figure 1J). Indeed, both lymphoma models exhibited dramatic splenomegaly (figure 1K), with a diffuse growth pattern and malignant expansion of GFP⁺ lymphoma B cells (figure 1C and L and online supplemental figure S1), corresponding to large plasmablastic cells (figure 1M) not terminally differentiated into CD138⁺ plasma cells (figure 1N).

Murine DEL-DLBCLs are primed for apoptosis

Overexpression of MYC can also lead to apoptosis,³² so that lymphomas tend to select for loss of TP53³³—already engineered in the pBIC and pBIC2 background (figure 2A,B)—or increased expression of BCL2/BCL-XL³⁴ in order to render malignant cells resistant to the deleterious effects of elevated MYC levels. To investigate the pro-survival effects of BCL2 upregulation and the

genomic instability leveraged by TP53 deficiency and MYC overexpression, we measured apoptosis initiation and DNA damage responses by flow cytometry after cryopreservation of murine lymphoma single-cell suspensions. In comparison to normal GC B cells, lymphoma GFP⁺ cells from both murine DEL-DLBCL models (ie, pBIC and pBIC2 mice) exhibited comparable reduced levels of AnnexinV and intracellular active caspase3 (figure 2C), indicating resistance to apoptosis, while they accumulated higher levels of phosphorylated histone 2AX (γH2AX) (figure 2D), demonstrating ongoing genotoxicity. Consistently, RNAseq and gene set enrichment analysis (GSEA) showed positive enrichment of MYC hallmarks and significant under-representation of the apoptosis transcriptional program in freshly FACS-sorted GFP⁺ pBIC or pBIC2 lymphoma cells (figure 2E).

However, some pro-apoptotic factors such as BAK1, PMAIP1, BCL11, BCL13 and BCL14 showed increased expression (figure 2F), suggesting certain level of apoptosis priming in tumor cells that may be efficiently repressed by acquiring BCL2 expression. To further explore whether a potentially primed apoptosis could be licensed through BCL2 inhibition, fresh primary pBIC and pBIC2 lymphomas were exposed to escalating doses of venetoclax during 24 hours ex vivo. Similar cell-killing activity of venetoclax was observed for both DEL-DLBCL mouse models ($EC_{50} \approx 6.4-6.8 \mu M$) compared with DMSO or refractory BCL2-negative GC B cells from control YC mice (figure 2G). This sensitivity to venetoclax was directly correlated to BCL2 expression (online supplemental figure S2), as previously described in human.³⁵ Furthermore, lymphoma cells induced the activation of caspase3 and the externalization of phosphatidylserine in response to BCL2 inhibition (figure 2H), confirming apoptosis as the expected cell death mechanism promoted by venetoclax.³⁵ Altogether, these results support the value of both pBIC mice (with spontaneous MYC/BCL2 expression) and pBIC2 mice (with spontaneous MYC expression but genetically enforced expression of BCL2) as comparable in vivo platforms to study the biology of DEL-DLBCL.

Combination of venetoclax with anti-CD20 immunotherapy demonstrates extended therapeutic benefit for DEL-DLBCL in vivo

To evaluate preclinically the potential of combination therapy with venetoclax for DEL-DLBCL, pBIC mice at advanced stages of the disease ($t=180$ days) were selected as better representative of spontaneous DEL-DLBCL and were randomized to be treated intraperitoneally with either venetoclax (250 μg two times a week) or anti-CD20 monoclonal antibody (10 mg/kg, 200 μg once a week) alone, or in combination, for 8 weeks. Overall survival

(OS) responses were superior in the combination group compared with anti-CD20 monotherapy, even though no significant improvement could be observed with the single venetoclax regimen (figure 3A). Accordingly, characterization of B-cell lymphomas by flow cytometry at 4 weeks after treatment initiation (half-time of treatment duration, $t=208$ days) revealed the complete clearance of both normal and GFP⁺ lymphoma B cells in the spleen of mice treated with anti-CD20 alone or in combination with venetoclax (figure 3B). Interestingly, the venetoclax group demonstrated specific killing of lymphoma cells (BCL2⁺ and primed for apoptosis) while sparing normal B cells (figure 3B); however, residual GFP⁺ tumors persisted and splenomegaly regression was less evident (figure 3C), likely explaining the failure of venetoclax to improve overall survival as monotherapy (figure 3A).

Venetoclax differentially affects tumor-infiltrating T-cell subsets in DLBCL

To investigate whether venetoclax could further contribute to antitumor activity in DLBCL through its recently revealed immunomodulatory activity on intra-tumoral T-cell subsets,^{17 18} we performed flow cytometry analysis of the immune cell populations within the TME of splenic lymphomas in regression after 4 weeks of treatment (half-time of treatment duration, $t=208$ days) (figure 3B,C). Consistent with human and murine DLBCL observations,^{19 36} untreated pBIC mice developed inflamed lymphomas highly infiltrated with CD8⁺ T cells (figure 4A and online supplemental figure S3A), where both CD8⁺ and CD4⁺ T cells predominantly expressed CD44 and PD-1 receptors (figure 4B and online supplemental figure S3B), suggesting increased T cell activation and tumor-antigen recognition. Supporting this tumor cognate state, CD44⁺PD-1⁺ T cells showed significantly higher IFN- γ level than their CD44PD-1⁻ neighbor

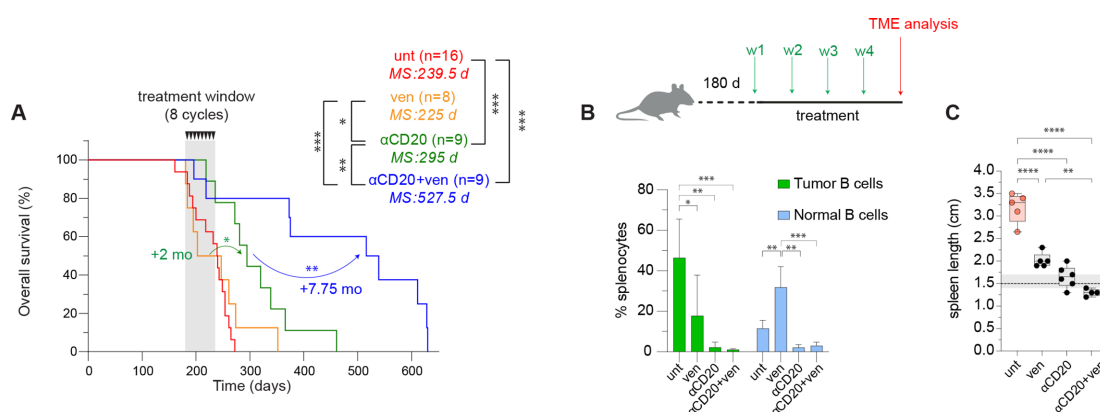


Figure 3 Combination of anti-CD20 immunotherapy and inhibition of BCL2 with venetoclax results in lymphoma reduction and prolonged survival in vivo. (A) Overall survival of pBIC mice that were untreated (receiving DMSO as vehicle), or treated with venetoclax (two i.p. weekly administrations of 250 μg), anti-CD20 (i.p. administration of 200 μg once a week) or the combination therapy, during a treatment window of 8 weeks (ie, 8 cycles). (B) Comparative percentages of CD19⁺GFP⁺ tumor cells and CD19⁺GFP⁻ normal B cells from pBIC lymphomas at half-time of the treatment duration (4 weeks as indicated in the scheme, $n \geq 3$). (C) Comparative spleen length of pBIC animals in response to the different treatment regimens, measured at half-time (4 weeks) of treatment duration. Reference for normal length of control YC spleens is marked with a horizontal line (mean) and gray fill (SD). Circle symbols represent individual animals. Log-rank (Mantel-Cox) tests and parametric t tests were used for statistical analysis: * $p \leq 0.05$, ** $p \leq 0.01$, *** $p \leq 0.001$, **** $p \leq 0.0001$. MS, median survival; TME, tumor microenvironment; ven, venetoclax.

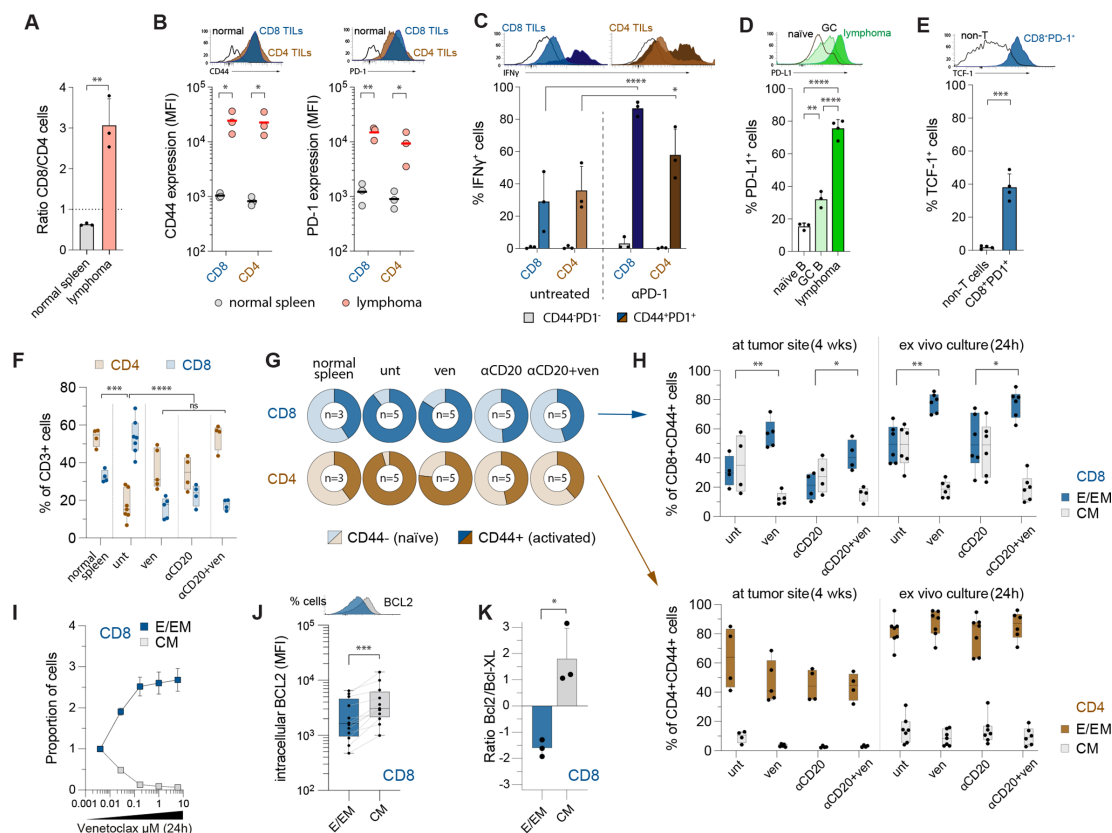


Figure 4 Systemic inhibition of BCL2 with venetoclax demonstrates immunomodulatory functions affecting the proportions of intratumoral T cells. (A) Comparative ratios of CD3⁺CD8⁺ over CD3⁺CD4⁺ T cells from normal murine spleens (n=3) and pBIC lymphomas at advanced stages of disease (n=3, ≥ 180 days). (B) Representative histograms and comparative expression by flow cytometry of CD44 and PD-1 surface markers, measured as median fluorescence intensity (MFI), within CD4 and CD8 T-cell compartments from control (n=3) or lymphoma pBIC mice (n=3). (C) Representative cytometry histograms and comparative percentages of IFN- γ ⁺ cells within adjacent naïve (CD44⁺PD-1⁻) or activated (CD44⁺PD-1⁺) CD4 and CD8 T-cell compartments that infiltrate untreated (n=3) or in vivo anti-PD-1-treated pBIC lymphomas (2 cycles of weekly i.p. treatment, n=3). (D) Representative cytometry histograms and comparative percentages of PD-L1⁺ B cells within normal B cell populations (naïve or GC B cells from YC control mice, n=3) or pBIC lymphomas (n=4). (E) Representative cytometry histograms and comparative percentages of TCF-1⁺ cells within CD8⁺PD-1⁺ T cells from pBIC lymphomas (n=4), using TCF-1 levels in paired adjacent non-T cells (CD3⁺GFP⁺) as negative controls. (F) Comparative fractions of CD3⁺CD4⁺ and CD3⁺CD8⁺ T cells from age-matched YC control mice and pBIC lymphomas in response to the different treatment regimens (n ≥ 3). (G) Pie charts showing percentages of CD8⁺ or CD4⁺ naïve T cells (CD44⁺CD62L⁺PD-1⁻) or antigen-primed and activated (CD44⁺) T cells in response to the different treatment regimens (n ≥ 3). (H) Comparative percentages of CD8⁺ (top) or CD4⁺ (bottom) effector/effector memory (E/EM, CD44⁺CD62L⁺PD-1⁺) and central memory (CM, CD44⁺CD62L⁺PD-1⁺) from pBIC lymphomas in response to the different in vivo treatment regimens (n ≥ 4 , left panels), or as measured ex vivo after culturing for 24 hours primary pBIC lymphomas obtained from moribund pBIC mice in the presence of the different treatments (n=7, right panels). (I) Relative proportions of E/EM and CM CD8⁺ T cells following 24 hours treatment with escalating doses of venetoclax (n=3). (J) BCL2 expression by intracellular flow cytometry in E/EM and CM CD8⁺ T cells as measured by MFI (n=10). (K) Comparative ratios of *Bcl2* over *Bcl-XL* expression in CD8⁺ E/EM and CM as determined by qRT-PCR (n=3). Log-rank (Mantel-Cox) tests, parametric t-tests, and non-linear fit analyses were used for statistical analysis: * $p \leq 0.05$, ** $p \leq 0.01$, *** $p \leq 0.001$, **** $p \leq 0.0001$.

counterparts, indicating greater cytotoxic potential (figure 4C, left). However, PD-1 is both a marker of activation but also of exhaustion,³⁷ and PD-L1 expressed by DLBCL cells in pBIC lymphomas (figure 4D) might suppress T-cell-mediated antitumor immune responses by engaging PD-1 on tumor-infiltrating lymphocytes (TILs). Supporting this notion, we had previously demonstrated that PD-1⁺ TILs in pBIC lymphomas exhibit exhaustion characteristics that may be overcome with in vivo PD-1 blockade immunotherapy.¹⁹ To gain further insight into the exhaustion state of CD44⁺PD-1⁺ T cells infiltrating

murine DEL-DLBCL tumors, we treated pBIC mice with anti-PD-1 monoclonal antibodies (10 mg/kg, 200 μ g once a week) for 2 weeks and evaluated potential changes in intracellular IFN- γ by cytometry. Compared with untreated mice, increased proportions of IFN- γ positive CD44⁺PD-1⁺ T cells could be observed after PD-1 blockade in both CD8⁺ and CD4⁺ compartments (figure 4C). Furthermore, transcription factor TCF-1, which is a key factor in anti-PD-1-responsive progenitor exhausted CD8⁺ T cells,^{38,39} was evidenced in pBIC CD8⁺PD-1⁺ T cells (figure 4E). These results support the presence of active

but attenuated antitumor T-cell functions in the murine lymphomas, where blockade of the PD-1/PD-L1 axis may restore partially exhausted effector functions of intratumoral CD44⁺PD-1⁺ T cells.

Consistent with successful lymphoma clearance and splenomegaly regression (figure 3B,C), all in vivo treatments targeting BCL2 or CD20 promoted the normalization of CD8/CD4 ratios (figure 4F) and the repopulation of the spleen with naïve T cells (CD44⁺CD62L⁺PD-1⁻) (figure 4G and online supplemental figure S4A). This restoration of the naïve T-cell compartment was especially evident for the most efficient anti-lymphoma regimens—involving anti-CD20 as monotherapy or in combination with venetoclax—reaching levels comparable to normal controls (online supplemental figure S3B). Subsequent assessment of effector-like features in the remaining intratumoral T cells, revealed that venetoclax led to a relative enrichment of CD8⁺ effector or effector-memory (E/EM, CD44⁺CD62L⁺PD-1⁺) cells at the tumors, which was, however, unnoticeable within the CD4 compartment, already significantly high in effector cells (figure 4H, left). This was further confirmed in ex vivo 2D co-cultures of heterogeneous primary murine lymphomas, which were exposed to the different treatments and demonstrated a relative enrichment of CD8⁺ E/EM cells already at 24 hours only in the presence of venetoclax (alone or in combination) (figure 4H, right, and online supplemental figure S3C). These observations could be explained by a direct effect of venetoclax specifically decreasing absolute numbers of CD8⁺ central memory (CM, CD44⁺CD62L⁺PD-1⁺) T cells (online supplemental figure S4B), which demonstrated a dose-dependent sensitivity to BCL2 inhibition (figure 4I), resulting in a proportional relative increase of resistant E/EM cells (figure 4H,I). This is strongly consistent with recent studies in human and colon cancer mouse models demonstrating that antigen-specific effector T cells tend to upregulate Bcl-XL expression and become more resistant to venetoclax than non-effector T cells (naïve and CM).¹⁸ Indeed, we could observe lower expression of BCL2 by intracellular cytometry (figure 4J) and inverted *Bcl2/Bcl-XL* ratios (figure 4K) in normal splenic E/EM cells compared with CM cells, supporting the reduced dependency of effector T cells on BCL2 for survival.

DISCUSSION

Double-expression of MYC and BCL2 provides adverse prognostic impact to DLBCL,^{1–5} which can be further complicated by TP53 loss.¹² The results described here support the value of pBIC mice¹⁹ as a preclinical in vivo model for these high risk DEL-DLBCL cases, and suggest that typical ABC-associated mutations that ultimately result in NF-κB activation, blockade of terminal B-cell differentiation and perturbation of TP53-mediated surveillance,^{24 40} can readily promote MYC/BCL2 co-expression and further contribute to GC-derived lymphomagenesis towards DLBCL. This is consistent with the

current proposed International Consensus Classification (ICC) of mature lymphoid neoplasms, which considers DEL-DLBCL as a phenotypic variant that would represent the end results of different biological pathways.² Whether enforced BCL2 expression can further accelerate disease was also investigated by crossing pBIC mice to *Eμ-hBCL2* transgenic mice (so-called pBIC2 mice), but the phenotypes were not altered significantly, indicating that activation of BCL2 is an early event in both spontaneous (pBIC) or BCL2-enforced (pBIC2) NF-κB-driven DEL-DLBCL lymphomagenesis.

Characterization of lymphoma progression in these multilesion mouse models by RNA-seq, flow cytometry and immunohistochemistry, provided evidences that acquisition of dual MYC and BCL2 expression during GC malignant transformation impairs apoptosis and allows the accumulation of genetic instability, hindering the clearance of malignant clones and facilitating the survival of DLBCL cells. In ex vivo conditions, these lymphoma cells remain intrinsically prone to cell death by the BCL2 inhibitor venetoclax, supporting the therapeutic potential of licensing apoptosis through BCL2 inhibition in DEL-DLBCL. Indeed, our pBIC mouse model provided a useful preclinical system to demonstrate that in vivo combination of anti-CD20 targeting and BCL2 inhibition results in synergistic anti-lymphoma effects, which at least in part can be explained by the specificity and pro-apoptotic effects of venetoclax against MYC/BCL2 co-expressing lymphoma B cells.

Another contribution of BCL2 targeting to the increased antitumor activity observed with anti-CD20 plus venetoclax was revealed by the altered T-cell phenotype observed in vivo and ex vivo on venetoclax treatment. Indeed, mature murine and human T cells have previously shown sensitivity to BCL2 inhibition, while Bcl-XL-dependent T-cell subsets such as more immature thymocytes or effector T cells are spared following treatment with venetoclax in vitro and in vivo.^{17 18} Consistent with this, analysis of pBIC lymphoma microenvironments by flow cytometry demonstrated a clear sensitivity of CD8⁺ central memory cells (CM, CD44⁺CD62L⁺PD-1⁺) to BCL2 inhibition, in contrast to a marked resistance and enrichment of CD8⁺ effector/effector memory cells (E/EM, CD44⁺CD62L⁺PD-1⁺). This venetoclax-mediated enrichment of intratumoral CD8⁺ T effector memory cells was also observed in a colon cancer syngeneic mouse model where it can augment the antitumor efficacy of PD-1/PD-L1 blockade in vivo.¹⁸ In the murine DEL-DLBCL microenvironment, CD44⁺PD-1⁺ T cells showed exhaustion features and failed to control the lymphoma in the late stage, but did respond to PD-1 blockade immunotherapy and exhibited expression of TCF-1, a transcription factor related to long-lived stem-like T-cell responses. Therefore, the resilience of PD-1⁺ activated effector T cells within pBIC lymphomas after venetoclax treatment, together with the striking reappearance of new potentially reactivable naïve T cells when lymphoma B cells are efficiently depleted by anti-CD20 antibodies, offer

a plausible opportunity for improved long-term anti-tumor immune responses and reduced or delayed risk of lymphoma relapse.

Current clinical data⁴¹ and our evidences here suggest that venetoclax monotherapy has limited efficacy in DLBCL, but combination therapy might improve therapeutic utility. Despite initial expectations,¹⁵ combination of venetoclax with more intense DA-EPOCH-R regimens appears excessively toxic and is not currently recommended.⁴² However, the improved responses that we see in the DEL-DLBCL pBIC mouse model when venetoclax is added to anti-CD20 immunotherapy, strongly support the improved efficacy that venetoclax plus conventional R/G-CHOP has demonstrated in first-line for DLBCL, particularly among patients with double-expressor status.^{13 14} Definitely, evaluation of this strategy in randomized trials (as in the currently ongoing NCT03984448) or in further combinations with immune checkpoint blockade (based on the impact of venetoclax on T-cell responses and the increasing relevance of PD-1/PD-L1 axis in DLBCL, postulated herein and in preclinical studies),^{18 19 36} offer novel promising opportunities for DLBCL patients.

Altogether, our data suggest that co-expression of MYC/BCL2 is an early pathogenic mechanism in NF- κ B-driven GC malignant transformation towards DEL-DLBCL. In this scenario, the specific BCL2 inhibitor venetoclax could efficiently cooperate with anti-CD20-based immunotherapy by providing two additional levels of antitumor protection: on the one hand, by licensing direct apoptosis of lymphoma cells that are intrinsically prone to constitutive NF- κ B/MYC-driven genotoxicity; and on the other hand, by enhancing antigen-specific effector T-cell responses through the restoration at the tumor site of a reactivable naïve T cell compartment and the preservation of activated effector CD8⁺ T cells that could enhance long-term control of DLBCL progression. These vulnerabilities of murine DEL-DLBCL to venetoclax provide relevant preclinical evidences to support further clinical investigation of novel immunotherapy combinations with BCL2 inhibitors in patients with high-risk DEL-DLBCL.

Author affiliations

¹Department of Biochemistry and Genetics, Universidad de Navarra, Pamplona, Spain

²Hemato-Oncology Program, Center for Applied Medical Research (CIMA), Pamplona, Spain

³Navarra Institute for Health Research (IdiSNA), Pamplona, Spain

⁴Department of Hematology, Clínica Universidad de Navarra, Pamplona, Spain

⁵Current address: Department of Hematology and Hemotherapy, Hospital Universitario Donostia, San Sebastián, Spain

⁶Department of Pathology, Universidad de Salamanca, Salamanca, Spain

⁷Bio-informatic Unit, Center for Applied Medical Research (CIMA), Pamplona, Spain

⁸Current address: Data Intelligence Unit, Techedge Spain, Madrid, Spain

⁹Department of Hematology-Oncology, Institut d'Investigacions Biomèdiques August Pi i Sunyer (IDIBAPS), Barcelona, Spain

¹⁰Centro de Investigación Biomédica en Red de Cáncer (CIBERONC), Instituto de Salud Carlos III, Madrid, Spain

Twitter Sergio Roa @Roa_Lab

Acknowledgements Authors acknowledge the excellent assistance provided for flow cytometry and cell sorting by Diego Alignani, for immunohistochemistry by the Morphology unit, and for animal husbandry by members of the Animal Facility, as well as for insightful discussions about T cell cancer immunology with Noelia Casares and Juan José Lasarte, all of them at Cima Universidad de Navarra. We are also indebted to Genentech for in vivo functional grade anti-mouse CD20 mAbs.

Contributors SR conceived the study and is guarantor; JM and SR designed experiments, analyzed and interpreted results, and cowrote the manuscript; JM, MG-L, SCG, AA-L and MP conducted experiments and/or analyzed data; CP contributed to the design and interpretation of preclinical trials; OB performed pathological analyses; VS and FJN performed bioinformatic analyses; JGV and PP-G contributed to the design and interpretation of ex vivo co-culture experiments; JAM-C contributed to the design and support of experiments, as well as to discussion of results; and all authors reviewed the manuscript.

Funding The study was funded by F. Hoffmann-La Roche through NAV4 imCORE project, as well as by grants to SR from Proyecto PID2020-112994RB-I00 financiado por MCIN/AEI /10.13039/501100011033, and Proyecto SAF2017-82309-R82309-R financiado por MCIN/AEI /10.13039/501100011033 y por FEDER Una manera de hacer Europa. Training support was received by Plan de Formación y de I+D 2019 from Gobierno de Navarra (Gobierno de Navarra 34E/2020) to JM, and by Ministerio de Universidades (FPU20/03256) to SCG. SR was supported by Ministerio de Economía y Competitividad through Programa Ramón y Cajal-I3 (RYC-2014-16399/MEC).

Competing interests SR has received research funding from Roche/Genentech (imCORE) and Gilead; JAM-C has received research funding from Roche/Genentech (imCORE) and Janssen Pharmaceuticals; CP has acted as a consultant for Roche, Janssen, Celgene/BMS and Kyowa Kirin. The remaining authors declare no conflicting financial interests.

Patient consent for publication Not applicable.

Ethics approval All animal handling and preclinical experiments were approved and conducted under the institutional guidelines of the University of Navarra Committee of Animal Experimentation (Ref: 085-19) and following the European Directive 2010/63/EU.

Provenance and peer review Not commissioned; externally peer reviewed.

Data availability statement Data are available in a public, open access repository. RNAseq files have been deposited in NCBI Gene Expression Omnibus and are accessible through GEO SuperSeries (GSE197693).

Supplemental material This content has been supplied by the author(s). It has not been vetted by BMJ Publishing Group Limited (BMJ) and may not have been peer-reviewed. Any opinions or recommendations discussed are solely those of the author(s) and are not endorsed by BMJ. BMJ disclaims all liability and responsibility arising from any reliance placed on the content. Where the content includes any translated material, BMJ does not warrant the accuracy and reliability of the translations (including but not limited to local regulations, clinical guidelines, terminology, drug names and drug dosages), and is not responsible for any error and/or omissions arising from translation and adaptation or otherwise.

Open access This is an open access article distributed in accordance with the Creative Commons Attribution Non Commercial (CC BY-NC 4.0) license, which permits others to distribute, remix, adapt, build upon this work non-commercially, and license their derivative works on different terms, provided the original work is properly cited, appropriate credit is given, any changes made indicated, and the use is non-commercial. See <http://creativecommons.org/licenses/by-nc/4.0/>.

ORCID iDs

Javier Melchor <http://orcid.org/0000-0003-1793-4152>
 Marcos Garcia-Lacarte <http://orcid.org/0000-0003-0614-8682>
 Sara C. Grijalba <http://orcid.org/0000-0003-4542-1805>
 Adrián Arnaiz-Leché <http://orcid.org/0000-0002-0687-0053>
 Marién Pascual <http://orcid.org/0000-0002-1678-1054>
 Carlos Panizo <http://orcid.org/0000-0002-3945-585X>
 Oscar Blanco <http://orcid.org/0000-0002-2667-0489>
 Víctor Segura <http://orcid.org/0000-0002-7740-6290>
 Francisco J. Novo <http://orcid.org/0000-0003-4961-3097>
 Juan García Valero <http://orcid.org/0000-0003-3193-9099>
 Patricia Pérez-Galán <http://orcid.org/0000-0003-3895-5024>
 Jose A. Martínez-Climent <http://orcid.org/0000-0002-7938-3950>
 Sergio Roa <http://orcid.org/0000-0003-1095-0715>

REFERENCES

- 1 Swerdlow SH, Campo E, Pileri SA, et al. The 2016 revision of the world Health organization classification of lymphoid neoplasms. *Blood* 2016;127:2375–90.
- 2 Campo E, Jaffe ES, Cook JR, et al. The International consensus classification of mature lymphoid neoplasms: a report from the clinical Advisory Committee. *Blood* 2022;140:1229–53.
- 3 Johnson NA, Slack GW, Savage KJ, et al. Concurrent expression of myc and Bcl2 in diffuse large B-cell lymphoma treated with rituximab plus cyclophosphamide, doxorubicin, vincristine, and prednisone. *J Clin Oncol* 2012;30:3452–9.
- 4 Staiger AM, Ziepert M, Horn H, et al. Clinical impact of the cell-of-origin classification and the MYC/Bcl2 dual expresser status in diffuse large B-cell lymphoma treated within prospective clinical trials of the German high-grade non-Hodgkin's lymphoma Study Group. *J Clin Oncol* 2017;35:2515–26.
- 5 Hu S, Xu-Monette ZY, Tzankov A, et al. MYC/BCL2 protein coexpression contributes to the inferior survival of activated B-cell subtype of diffuse large B-cell lymphoma and demonstrates high-risk gene expression signatures: a report from the International DLBCL rituximab-CHOP Consortium program. *Blood* 2013;121:quiz 4250:4021–31; .
- 6 Alizadeh AA, Eisen MB, Davis RE, et al. Distinct types of diffuse large B-cell lymphoma identified by gene expression profiling. *Nature* 2000;403:503–11.
- 7 Green TM, Young KH, Visco C, et al. Immunohistochemical double-hit score is a strong predictor of outcome in patients with diffuse large B-cell lymphoma treated with rituximab plus cyclophosphamide, doxorubicin, vincristine, and prednisone. *J Clin Oncol* 2012;30:3460–7.
- 8 Scott DW, Mottok A, Ennishi D, et al. Prognostic significance of diffuse large B-cell lymphoma cell of origin determined by digital gene expression in formalin-fixed paraffin-embedded tissue biopsies. *J Clin Oncol* 2015;33:2848–56.
- 9 Chapuy B, Stewart C, Dunford AJ, et al. Molecular subtypes of diffuse large B cell lymphoma are associated with distinct pathogenic mechanisms and outcomes. *Nat Med* 2018;24:679–90.
- 10 Xu-Monette ZY, Wu L, Visco C, et al. Mutational profile and prognostic significance of TP53 in diffuse large B-cell lymphoma patients treated with R-CHOP: report from an international DLBCL rituximab-CHOP Consortium program study. *Blood* 2012;120:3986–96.
- 11 Young KH, Leroy K, Møller MB, et al. Structural profiles of TP53 gene mutations predict clinical outcome in diffuse large B-cell lymphoma: an international collaborative study. *Blood* 2008;112:3088–98.
- 12 Meriranta L, Pasanen A, Alkods A, et al. Molecular background delineates outcome of double protein expressor diffuse large B-cell lymphoma. *Blood Adv* 2020;4:3742–53.
- 13 Zelenetz AD, Salles G, Mason KD, et al. Venetoclax plus R- or G-CHOP in non-Hodgkin lymphoma: results from the CAVALLI phase 1B trial. *Blood* 2019;133:1964–76.
- 14 Morschhauser F, Feugier P, Flinn IW, et al. A phase 2 study of venetoclax plus R-CHOP as first-line treatment for patients with diffuse large B-cell lymphoma. *Blood* 2021;137:600–9.
- 15 Rutherford SC, Abramson JS, Bartlett NL, et al. Venetoclax with dose-adjusted EPOCH-R as initial therapy for patients with aggressive B-cell lymphoma: a single-arm, multicentre, phase 1 study. *Lancet Haematol* 2021;8:e818–27.
- 16 Marsden VS, Strasser A. Control of apoptosis in the immune system: Bcl-2, BH3-only proteins and more. *Annu Rev Immunol* 2003;21:71–105.
- 17 Khaw SL, Méroin D, Anderson MA, et al. Both leukaemic and normal peripheral B lymphoid cells are highly sensitive to the selective pharmacological inhibition of prosurvival Bcl-2 with ABT-199. *Leukemia* 2014;28:1207–15.
- 18 Kohlhapp FJ, Haribhai D, Mathew R, et al. Venetoclax increases intratumoral effector T cells and antitumor efficacy in combination with immune checkpoint blockade. *Cancer Discov* 2021;11:68–79.
- 19 Pascual M, Mena-Varas M, Robles EF, et al. Pd-1/Pd-L1 immune checkpoint and p53 loss facilitate tumor progression in activated B-cell diffuse large B-cell lymphomas. *Blood* 2019;133:2401–12.
- 20 Strasser A, Whittingham S, Vaux DL, et al. Enforced Bcl2 expression in B-lymphoid cells prolongs antibody responses and elicits autoimmune disease. *Proc Natl Acad Sci U S A* 1991;88:8661–5.
- 21 Reddy A, Zhang J, Davis NS, et al. Genetic and functional drivers of diffuse large B cell lymphoma. *Cell* 2017;171:481–94.
- 22 Scholze H, Stephenson RE, Reynolds R, et al. Combined EZH2 and Bcl-2 inhibitors as precision therapy for genetically defined DLBCL subtypes. *Blood Adv* 2020;4:5226–31.
- 23 Shaffer AL 3rd, Young RM, Staudt LM. Pathogenesis of human B cell lymphomas. *Annu Rev Immunol* 2012;30:565–610.
- 24 Ennishi D, Hsi ED, Steidl C, et al. Toward a new molecular taxonomy of diffuse large B-cell lymphoma. *Cancer Discov* 2020;10:1267–81.
- 25 La Rosa FA, Pierce JW, Sonenshein GE. Differential regulation of the c-myc oncogene promoter by the NF-kappa B rel family of transcription factors. *Mol Cell Biol* 1994;14:1039–44.
- 26 Ji L, Arcinas M, Boxer LM. Nf-Kappa B sites function as positive regulators of expression of the translocated c-myc allele in Burkitt's lymphoma. *Mol Cell Biol* 1994;14:7967–74.
- 27 Catz SD, Johnson JL. Transcriptional regulation of Bcl-2 by nuclear factor kappa B and its significance in prostate cancer. *Oncogene* 2001;20:7342–51.
- 28 Grossmann M, O'Reilly LA, Gugasyan R, et al. The anti-apoptotic activities of Rel and RelA required during B-cell maturation involve the regulation of Bcl-2 expression. *EMBO J* 2000;19:6351–60.
- 29 Calado DP, Zhang B, Srinivasan L, et al. Constitutive canonical NF-kB activation cooperates with disruption of Blimp1 in the pathogenesis of activated B cell-like diffuse large cell lymphoma. *Cancer Cell* 2010;18:580–9.
- 30 Calado DP, Sasaki Y, Godinho SA, et al. The cell-cycle regulator c-myc is essential for the formation and maintenance of germinal centers. *Nat Immunol* 2012;13:1092–100.
- 31 Shen Y, Iqbal J, Huang JZ, et al. BCL2 protein expression parallels its mrna level in normal and malignant B cells. *Blood* 2004;104:2936–9.
- 32 Hoffman B, Liebermann DA. Apoptotic signaling by c-MYC. *Oncogene* 2008;27:6462–72.
- 33 Eischen CM, Weber JD, Roussel MF, et al. Disruption of the ARF-mdm2-p53 tumor suppressor pathway in myc-induced lymphomagenesis. *Genes Dev* 1999;13:2658–69.
- 34 Eischen CM, Woo D, Roussel MF, et al. Apoptosis triggered by myc-induced suppression of bcl-X(L) or bcl-2 is bypassed during lymphomagenesis. *Mol Cell Biol* 2001;21:5063–70.
- 35 Souers AJ, Leverson JD, Boghaert ER, et al. ABT-199, a potent and selective BCL-2 inhibitor, achieves antitumor activity while sparing platelets. *Nat Med* 2013;19:202–8.
- 36 Garcia-Lacarte M, Grijalba SC, Melchor J, et al. The PD-1/PD-L1 checkpoint in normal germinal centers and diffuse large B-cell lymphomas. *Cancers (Basel)* 2021;13:4683.
- 37 Sharpe AH, Pauken KE. The diverse functions of the PD1 inhibitory pathway. *Nat Rev Immunol* 2018;18:153–67.
- 38 Siddiqui I, Schaeuble K, Chennupati V, et al. Intratumoral tcf1+PD-1+CD8+ T cells with stem-like properties promote tumor control in response to vaccination and checkpoint blockade immunotherapy. *Immunity* 2019;50:195–211.
- 39 Kurtulus S, Madi A, Escobar G, et al. Checkpoint blockade immunotherapy induces dynamic changes in PD-1–CD8+ tumor-infiltrating T cells. *Immunity* 2019;50:181–194.
- 40 Wright GW, Huang DW, Phelan JD, et al. A probabilistic classification tool for genetic subtypes of diffuse large B cell lymphoma with therapeutic implications. *Cancer Cell* 2020;37:551–68.
- 41 Davids MS, Roberts AW, Seymour JF, et al. Phase I first-in-human study of venetoclax in patients with relapsed or refractory non-Hodgkin lymphoma. *J Clin Oncol* 2017;35:826–33.
- 42 Abramson JS, Ruppert AS, Giri S, et al. Randomized phase II/III study of DA-EPOCH-R +/- venetoclax in previously untreated double hit lymphoma: initial results from alliance A051701. *Blood* 2021;138(Supplement 1):523.